第 32 卷第 1 期 无 机 化 学 学 报 Vol.32 No.1
2016 年 1 月 CHINESE JOURNAL OF INORGANIC CHEMISTRY 25-33

一种电荷转移晶体的磁和介电弛豫性质

张雪梅[1] 于姗姗[2] 张 辉[2] 段海宝*,[2]
([1]安徽科技学院化学与材料工程学院,蚌埠 233100)
([2]南京晓庄学院环境科学学院,南京 211171)

摘要:在外加电场下,利用分子的旋转和取向运动是组装分子介电马达以及弛豫型分子介电体的一个主要策略。在本论文中,我们制备并表征了一个新的电荷转移晶体[C_{10}-DMPy][Ni(mnt)$_2$](**1**)(C_{10}-DMPy$^+$=1-decanel-*N*, *N*-dimethylpyridinium, mnt^{2-}=马来二氰基二硫烯)。在一定的频率范围内,该化合物展现了介电弛豫行为,我们将此归于平衡阳离子的动力学位置取向和阴、阳离子间的电荷转移。该化合物的介电弛豫过程遵循 Cole-Cole 方程,偏离理想的 Debye 模型。单晶 X-射线衍射表明该化合物的阴、阳离子分别独立堆积成柱状,柔性的有机阳离子与刚性的磁性阴离子构筑块间存在电荷协助氢键作用。此外,该化合物的磁行为展现为弱的铁磁耦合作用。

关键词:电荷转移晶体;晶体结构;介电响应;磁性质
中图分类号:O614.81$^+$3 **文献标识码**:A **文章编号**:1001-4861(2016)01-0025-09
DOI:10.11862/CJIC.2016.002

Magnetic and Relax-like Dielectric Response Behavior in a Charge-Transfer Crystal

ZHANG Xue-Mei[1] YU Shan-Shan[2] ZHANG Hui[2] DUAN Hai-Bao*,[2]
([1]*School of Chemical and Material Engineering, Anhui Science and Technology University, Bengbu, Anhui* 233100, *China*)
([2]*School of Environmental Science, Nanjing Xiaozhuang University, Nanjing* 211171, *China*)

Abstract: Molecular rotation and orientation by applied electric field is one of the promising strategies for assembling the potential molecular dielectric rotors and relax-like dielectric. Here, a new charge transfer compound [C_{10}-DMPy][Ni(mnt)$_2$] (**1**) (C_{10}-DMPy$^+$=1-decanel-*N*, *N*-dimethylpyridinium cation, mnt^{2-}=maleonitriledithiolate), which shows interesting dielectric relaxation process, is synthesized and characterized. The anions and cations of **1** are aligned into segregated stacks. There existed weakly charge-assisted hydrogen bonding interactions between the mobile organic cation and rigid [Ni(mnt)$_2$]$^-$ anion. Large temperature-dependent dielectric constant values and dielectric relaxation process of **1** can be ascribed to the dynamic orientation motion of alkyl chain of the organic cation and charge transfer between anions and cations. The overall magnetic behavior of **1** corresponds to a paramagnetic system with ferromagnetic coupling interaction. CCDC: 1415204, **1**.

Keywords: charge-transfer crystal; crystal structure; dielectric response; magnetic properties

Relaxation means a systems monotonous approach to the equilibrium state after some excitation. In the case of dielectric relaxation one considers the response of polarization to an external alternating current field. Dielectric relaxation spectroscopy can provides information about the orientation adjustment of mobile charge present in the dielectric medium[1-3]. The dielectric relaxation methods are commonly used

收稿日期:2015-07-27。收修改稿日期:2015-10-16。
国家自然科学基金(No.21201103,21301093)资助项目。
*通信联系人。E-mail:duanhaibao4660@163.com

in studies of ionic conductivity and molecular dynamics in different dielectric materials, such as glasses, crystal and liquids[4-7]. It is well known that the measurements of alternating current (ac) conductivity can provide the underling mechanisms of the dielectric relaxation[8-10].

In general, molecular rotation and orientation by applied electric field is one of the promising strategies for assembling the potential molecular ferroelectric and switchable dielectric[11-16]. Approaches to creating such materials with internal reorientation or rotation include molecular crystal with rotary groups [17-18], inclusion compounds with rotating guests and rotor-coated surfaces[19-21]. In our previous studies, a series of ion-pair compounds with spin-Peierls-type transition were achieved, which consist of bis(maleonitriledithio) metalate monoanion (abbr. $[M(mnt)_2]^-$ and M=Ni or Pt) bearing $S=1/2$ spin and organic cation with tunable molecular conformation[22-24]. Recently, we explored to introduce mobile organic cation into the rigid $[Ni(mnt)_2]^-$ spin system and created a bifunctional compound[25]. Further investigation indicated utilization of such rigid $[Ni(mnt)_2]^{2-}$ molecular block as a stator unit can create a switchable dielectrics. However, there are a limited number of studies on the dielectric relaxation and ac conductivity of $[Ni(mnt)_2]^-$ spin system. Theses compounds may show interesting dielectric features. Usually, there are weakly charge-assisted interactions between the mobile organic cation and rigid $[Ni(mnt)_2]^-$ anion, and the dipole motion of the cations under an ac electrical field may give rise to an interesting dielectric response.

Encouraged by our previous study and above-mentioned findings, in this paper, we present a new compound $[C_{10}\text{-DMPy}][Ni(mnt)_2]$(**1**) ($C_{10}$-DMPy$^+$=1-decanel-*N*, *N*-dimethylpyridinium cation, mnt^{2-}=maleonitriledithiolate). This compound showed novel dielectric relaxation behaviors.

1 Experimental

1.1 Chemicals and reagents

All reagents and chemicals were purchased from commercial sources and used without further purification. The starting materials disodium maleonitriledithiolate (Na_2mnt) and 1-decanel-*N*, *N*-dimethylpyridinium bromide were synthesized following the published procedures[26-27].

1.2 Physical measurements

Elemental analyses (C, H and N) were performed with an Elementar Vario EL Ⅲ analytical instrument. IR spectra were recorded on a Bruker Vector 22 Fourier Transform Infrared Spectrometer (170SX) (KBr disc). Differential scanning calorimetry (DSC) experiments for **1** were carried out on a Pyris 1 power-compensation differential scanning calorimeter and the heating-cooling treatments were performed up to two cycles with the heating/cooling rate of 10 K·min^{-1}. Magnetic susceptibility data on polycrystalline-sample were collected over the temperature range of 1.8~400 K for **1** using a Quantum Design MPMS-5 superconducting quantum interference device (SQUID) magnetometer. Temperature and frequency dependent dielectric constant, ε, dielectric loss, tanδ, the impedance, Z, and ac conductivity, σ(ac) measurements were carried out employing Concept 80 system (Novocontrol, Germany); the powdered pellet, which was prepared under 10 MPa pressure, and was coated by gold films on the opposite surfaces and was sandwiched by the copper electrodes. The pellet had a thickness of *ca.* 0.80 mm and 78.5 mm^2 in the area. The rang of the ac frequencies was 1~10^7 Hz.

1.3 Preparations for 1

Na_2mnt (2.0 mmol) and $NiCl_2\cdot 6H_2O$ (1.0mmol) were mixed under stirring in MeOH. Subsequently, a CH_3CN solution of 1-decanel-*N*, *N*-dimethylpyridinium bromide (2.0 mmol) was added, and the red precipitate was washed with MeOH. A MeOH solution with I_2 (0.40 mmol) was added to the mixture; the mixture was allowed standing overnight after stirred for 25 minutes. The black precipitate formed were filtered off, washed with MeOH and dried at 65 ℃ in vacuum to give compound **1**. Yield: ~42%.

The single crystals suitable for X-ray analysis were obtained by evaporation of the corresponding compound in MeOH to give black-needle crystals for **1**.

1.4 X-ray crystallography

The diffraction data for single crystals were collected with graphite monochromated Mo $K\alpha$ (λ = 0.071 073 nm) on a CCD area detector (Bruker-SMART). Data reductions and absorption corrections were performed with the SAINT and SADABS software packages [28], respectively. Structures were solved by the direct method and refined by the full-matrix least-squares procedure on F^2 using SHELXL-97 program[29]. The non-hydrogen atoms were refined anisotropically, and the hydrogen atoms were introduced at calculated positions (C-H 0.093 0 nm for benzene and 0.097 0 nm for methylene) and refined riding on the parent atoms with U(H)=1.2Ueq (bonded C or N atoms). The crystallographic details about data collection and structural refinement are summarized in Table 1. Selected bond lengths and angles together with their estimated standard deviations are listed in Table 2.

CCDC: 1415204, **1**.

Table 1　Crystal data and structural refinements at 293 K for 1

Compounds	**1**	V / nm^3	1.461 5(7)
Empirical formula	$C_{25}H_{31}N_6NiS_4$	D_c / (g·cm^{-3})	1.369
Crystal system	Triclinic	μ / mm^{-1}	0.975
Space group	$P\bar{1}$	F(000)	630.0
a / nm	0.982 63(13)	Limiting indices	$-12\leqslant h\leqslant 12$; $-14\leqslant k\leqslant 13$; $-18\leqslant l\leqslant 18$
b / nm	1.141 94(19)	θ range for data collection / (°)	1.79~27.46
c / nm	1.388 3(1)	Reflections collected	6 613
α / (°)	99.316(2)	Independent reflections	4 506
β / (°)	105.995(2)	Goodness of fit on F^2	1.021
γ / (°)	95.581(2)	R_1, wR_2 [$I>2\sigma(I)$]	0.044 0, 0.122 1

Table 2　Selected bond lengths (nm) and bond angles (°) for 1

Ni(1)-S(1)	0.215 25(8)	Ni(1)-S(2)	0.215 84(8)	Ni(1)-S(3)	0.214 88(8)
Ni(1)-S(4)	0.214 68(8)	S(1)-C(2)	0.172 1(3)	S(2)-C(3)	0.172 7(3)
S(3)-C(6)	0.171 8(3)	S(4)-C(7)	0.171 6(3)	N(1)-C(1)	0.114 9(4)
N(2)-C(4)	0.113 9(3)	N(3)-C(5)	0.113 8(4)	N(4)-C(8)	0.144 7(5)
S(1)-Ni(1)-S(2)	92.68(3)	S(3)-Ni(1)-S(2)	179.59(3)	S(4)-Ni(1)-S(2)	87.76(3)
S(3)-Ni(1)-S(1)	87.32(3)	C(2)-S(1)-Ni(1)	103.15(10)	C(3)-S(2)-Ni(1)	103.10(10)
C(19)-N(5)-C(23)	118.4(2)	C(19)-N(5)-C(18)	122.0(3)	C(23)-N(5)-C(18)	119.6(3)
C(21)-N(6)-C(24)	117.4(4)				

2 Results and discussion

2.1 Crystal structure

Compound **1** crystallizes in triclinic space group $P\bar{1}$ at room temperature, as shown in Fig.1a, and an asymmetry unit is comprised of a pair of $[Ni(mnt)_2]^-$ anion and C_{10}-DMPy$^+$ cation. The $[Ni(mnt)_2]^-$ anions possess an approximated planar geometry, and the mean-molecule-plane of $[Ni(mnt)_2]^-$ anion, defined through four coordinated S atoms, makes a dihedral angle of 2.9° with the pyridine ring in the cation. The bond lengths and angles are in good agreement with the reported $[Ni(mnt)_2]^-$ compounds [22-23]. The cations exhibit different alkyl chain conformation, namely, from C11 to C19 atoms show completely trans-planar conformation in the hydrocarbon chain, whereas the C9 and C10 atoms in the pyridyl ring tail display a *cis* conformation. The direction of alkyl chain is

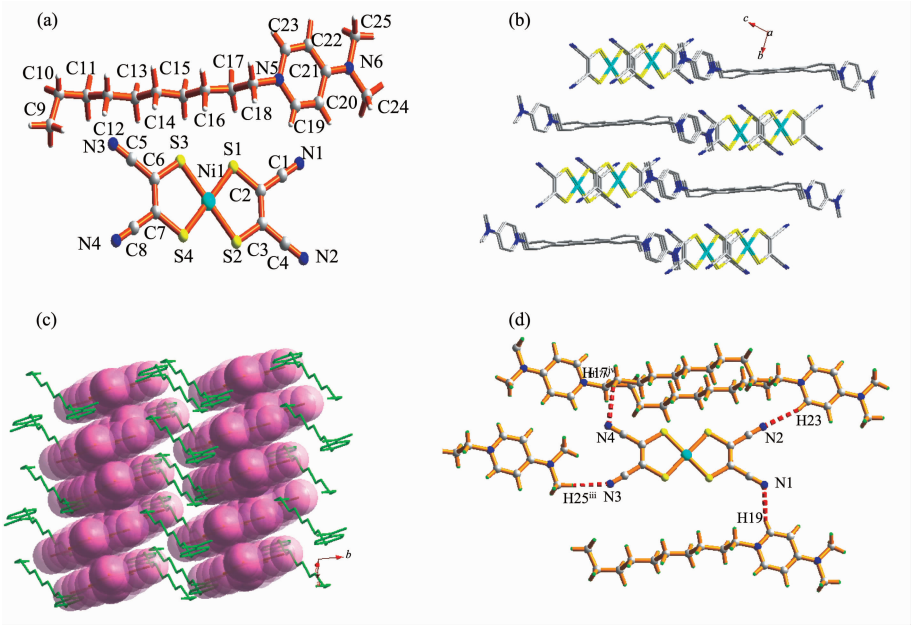

Fig.1 (a) ORTEP view labelling atom and thermal ellipsoids drawn at the 20% probability level for **1**;(b) Packing structure of **1** viewed along the a axis;(c) The layer arrangement parallel to the (111) plane, showing the alternating stacks of anions and cations; (d) Anionic dimer with the longitudinal offset mode (Symmetry code: [iii] 1−*x*, 0.5+*y*, *z*; [iv] −*x*, 1−*y*, −1+*z*).

almost parallel to the long molecular axis of $[Ni(mnt)_2]^-$ anions. All the alkyl of the cations are nor disordered at room temperature.

As shown in Fig.1b and 1c, the anions and cations are aligned into segregated stacks, respectively. The two neighboring $Ni[(mnt)_2]^-$ anions are formed into π-type dimer along the crystallographic *a* axis direction with the shorter interatomic separations is 0.3995 nm of Ni(1)⋯Ni(1)[i] (Symmetry code: [i]*x*, −1 +*y*, *z*). The adjacent anions dimers with a slippage arrangement along both short and long molecular axes of the anions form a zigzag chain. Each anions chain was surrounded by four nonmagnetic cations stacks. There existed charge assisted C-H⋯N and N-H⋯N interactions between the adjacent anion and cation stacks, as demonstrated in Fig.1d, the shorter inter-atomic contacts are found (C(19)⋯N(1) 0.331 8 nm, H(19)⋯N(1) 0.256 8 nm, C(19)-H(19)⋯N(1) 146.75°, C(23)[ii]⋯N(2) 0.351 4 nm, H(23)⋯N(2) 0.265 2 nm, C(19)-H(19)⋯N(1) 161.19°, N(25)[iii]⋯N(3) 0.352 3 nm, H(25A)⋯N(3) 0.255 7 nm, C(19)-H(19)⋯N(1) 175.14°, C(17)[iv]⋯N(4) 0.349 6 nm, H(17B)⋯N(4) 0.272 8 nm, C(19)-H(19)⋯N(1) 138.57° (Symmetry code: [ii]*x*, *y*, −1+*z*; [iii]1−*x*, 0.5+*y*, *z*; [iv]−*x*, 1−*y*, −1 +*z*). Along the *c* axis direction, two C_{10}-DMPy$^+$ cations are arranged in an anti-parallel arrangement, a longer centroid-to-centroid separation (0.680 750 nm) of pyridine owing to the steric hindrance between the *N*,*N*-dimethyl groups and the alkyl chain. The cations are further arranged into the individual cation layers, which are also parallel to the *ab*-plane.

2.2 Magnetic property of 1

The plots of χ_m as a function of temperature of **1** in the temperature range of 1.8~400 K is displayed in Fig.2, where χ_m represents the molar magnetic susceptibility with one $[Ni(mnt)_2]^-$ per formula unit and

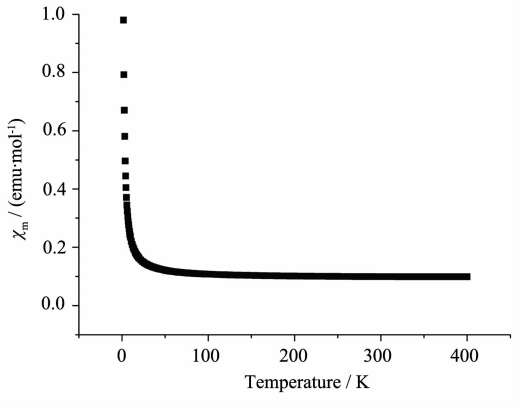

Fig.2 Plots of χ_m-*T* for **1**

the diamagnetism contributed from the atomic cores was not removed. The overall magnetic behavior of **1** corresponds to a paramagnetic system with ferromagnetic coupling interaction.

The $\chi_m T$ value at 300 K is 0.390 emu·K·mol^{-1} which is slightly higher than the spin-only value expected for system with S=1/2 (0.375 emu·K·mol^{-1}). With the temperature decrease, the value of χ_m slightly increases. Below 25 K, the χ_m values decrease steeply, and such the typical Curie paramagnetic behavior of **1** in low temperature region arises from the magnetic impurity caused by the lattice defects. In order to estimate the magnetic exchange nature of 1, the simple Curie-Weiss law was used to analyze the magnetic susceptibility data over the range of 1.8~ 400 K:

$$\chi_m = \frac{C}{T-\theta} + \chi_0 \qquad (1)$$

where the symbols of χ_0 is contributed by the core diamagnetism and the possible temperature-independent van Vleck-type paramagnetic susceptibility originated from the coupling of the ground and excited states through a magnetic field, and then C/T term represents the paramagnetism from the magnetic impurity. However, the obtained C values from fits are too large and seem unreasonable. The inability of Curie-Weiss models to describe the magnetic behavior indicates this 1-D spin system probably posses strong magnetic anisotropy, which leads to the temperature dependent magnetic susceptibility deviating from the isotropic magnetic coupling model.

2.3 Dielectric properties

The relative permittivity $\varepsilon^*(\omega)$ of the dielectric material as function of frequency is given by:

$$\varepsilon^*(\omega) = \varepsilon'(\omega) - i\varepsilon''(\omega) \qquad (2)$$

Frequency dependent of the dielectric permittivity ε' and dielectric loss $\tan\delta=\varepsilon''/\varepsilon'$ for **1** are shown in Fig.3 in the temperature range of 50~130 ℃. From the Fig.3, it can be seen that the values ε' rapidly drops from about 40 to 7 with the increase of the field frequency from 1 to 10^4 Hz at 130 ℃. The nature of the dielectric permittivity related to oscillating free dipoles (like long alkyl chain of the organic cation) in an alternating field. At very low frequencies, the dipoles motion can follow the applied electric field. As the frequency increases and reaches a characteristic value ($\omega=1/\tau$), the dielectric constant slightly decreases and exhibit relaxation process. The different model of mechanisms leads to the resonance dielectric relaxation spectra in the case of electronic polarization or molecular vibrations which occur at frequency beyond 10^{12} Hz. Below this frequency, the dielectric relaxation spectra prevail relating to the behavior of dipole motion or ionic polarization. For **1**, $[Ni(mnt)_2]^-$ anions have rigid planar configuration and the motion at small electric field is very difficult. Therefore, the relaxation that appears in 1 ~10^4 Hz could be attributed to dipole motion of the organic cations in **1**. Dielectric relaxation process were also observed in the tanδ-f plot (Fig.3b). The dielectric relaxation spectra of **1**, transformed into electric modulus spectra in Fig.4a by using Eq. (**3**), the dielectric modulus representation minimizes the unwanted effects of the extrinsic relaxation and is often used in the analysis of the dynamic conductivity of solids[30]. It can essentially eliminate the problem of

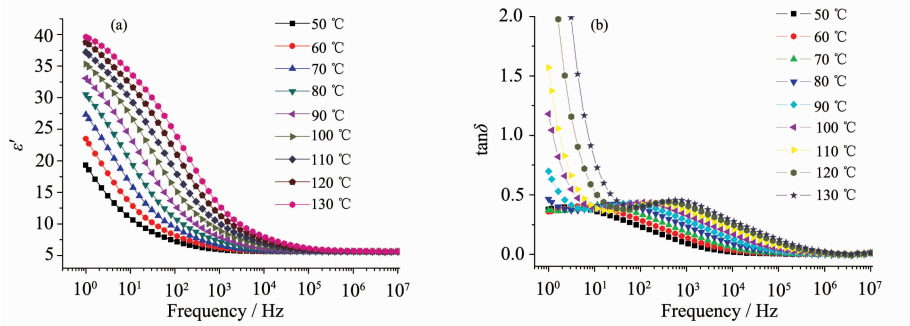

Fig.3　Frequency dependences of ε'(a) and tanδ (b) for **1** in the range of 50~130 ℃

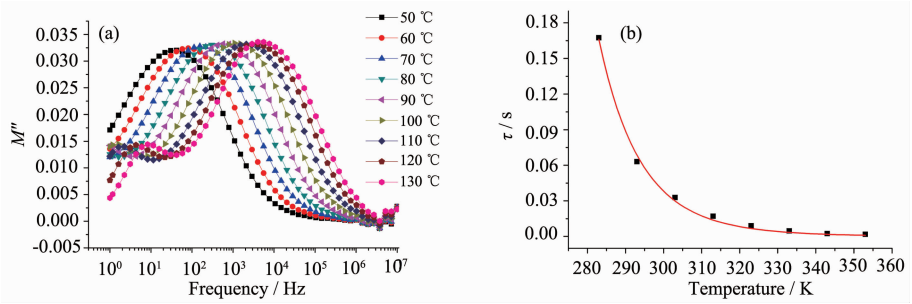

Fig.4 Frequency dependences of dielectric modulus M'' (a) and plots of τ versus T for **1** (b) at selected temperature

the electrode polarization and space charge injection phenomena.

$$M'(\omega) = \frac{\varepsilon'}{\varepsilon'^2+\varepsilon''^2} \qquad M''(\omega) = \frac{\varepsilon''}{\varepsilon'^2+\varepsilon''^2} \tag{3}$$

It is observed that the maximum in M″ peak shift to higher frequency with the temperature increase. In the frequency region below peak maximum, the charge carrier drifts to long distance. For the frequency above peak maximum M'', the carrier seem to be confined to potential well, thus drifts to short distances or spatially localized. In order to get the deep insight into the dielectric relaxation process, the frequency-dependence of peak for the dielectric loss at different temperature is plotted (Fig.4b) and the following relation is:

$$\tau = \tau_0 \exp\left(\frac{E_a}{k_B T}\right) \tag{4}$$

Where $\tau=1/f_{max}$ and f_{max} is the frequency at maximum in the plot of tanδ-f under a selected temperature; τ_0 represents the characteristic macroscopic relation time, E_a is the activation energy or potential barrier required for the dielectric relaxation, k_B is Boltzmanns constant. The best fits giving the following results using Eq.(**4**): τ_0=8.928(3)×10^{-13} s and E_a=0.63(1) eV. According to our previous work, this dielectric relaxation is attributed to dynamic orientation motion segmental motions of the organic cation. Similar relaxation have been reported in polymer. The E_a and τ_0 values in this compound are slightly larger than our reported compound 1,10-bis(1-methylimidazolium)decane bis (maleonitriodithiolato) nickelate[31]. For this compound, the segregated stacks of anions and cations and diverse charge-assisted H⋯N, C⋯N and H⋯S interactions between the adjacent anion and cation stacks (as shown in Fig.1d) stabilize the cations in its lattice, furthermore, the rigid pyridine ring compared to imidazolyl ring in **1** give seldom freedom for the motion of the cations, which may be the reason for its relatively larger activation energy and τ_0.

Carefully check the temperature dependence dielectric constant (ε'') and dielectric loss (tanδ) at selected frequency for **1** (Fig.5a and 5b), the second step dielectric relaxation was observed in the range of 50~110 ℃ and at the frequency from 10^5 to 10^6 Hz. The dielectric constant and loss are almost constants at low temperature. With the temperature increasing,

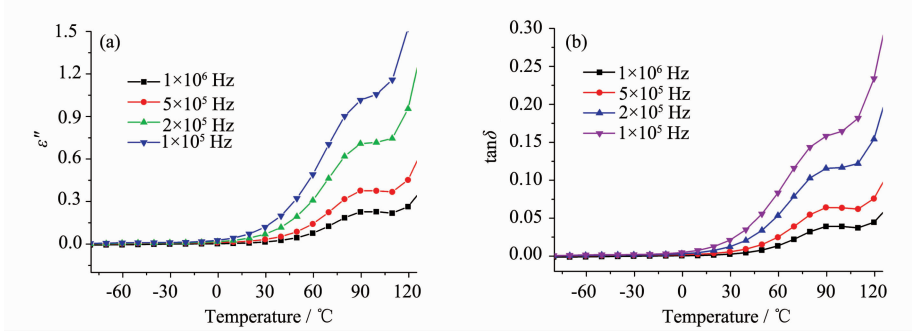

Fig.5 Temperature dependences of ε''(a) and tanδ (b) for **1** at the selected frequency

the wide dielectric loss and constant peak become visible in the range of 50~110 ℃ and maxima of all peaks shift toward high frequencies. This dielectric behavior is typical thermal assisted dielectric relaxation, and may be related to charge transfer of the cations and anions. At high frequencies (10^5 to 10^6 Hz), the dipoles motion (organic cation segments motion, the first step dielectric relaxation) cannot follow the applied electric field, and second relaxation becomes apparent.

The relaxation process for **1** at selected temperatures was fitted using Cole-Cole model function:

$$\varepsilon^* = \varepsilon' - i\varepsilon'' = \varepsilon_\infty + \frac{\varepsilon_0 - \varepsilon_\infty}{1+(i\omega\tau)^{1-\alpha}} \quad (5)$$

Where the symbols ε_0 and ε_∞ are respectively the static and high frequencies limits of dielectric permittivity, is relaxation time related to the frequency of maximum dielectric loss and is parameter which describe the shape of the relaxation spectra with the range of 0~1. For an ideal Debye relaxation, α=0. Fig.6 shows the Cole-Cole plots of the

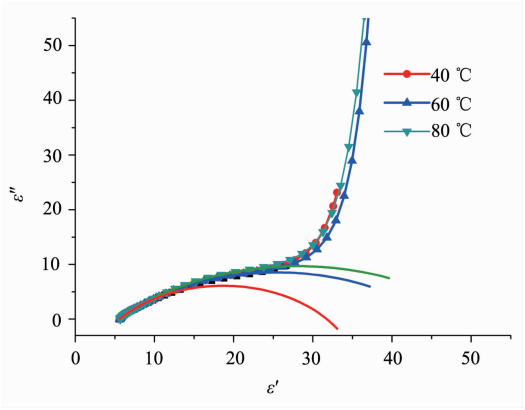

Fig.6　Plots of ε'' versus ε' at selected temperatures for **1** (Open: experimental data; lines: theoretically reproduced using Eq.(**5**)).

relaxation process for **1** at selected temperatures, and the best fits using Eq.(**5**) for the plots of ε"-ε yielded the corresponding parameters ε_0, ε_∞ and α for **1**, which are summarized in Table 3. The fitted ε_∞ parameter is closed to the dielectric constant at higher frequency (f>10^5 Hz) for **1**, and the fitted α parameters deviate from zero, indicating that the relaxation process depart from the ideal Debye dielectric response.

Table 3　ε_0, ε_∞ and α parameters for 1

Temperature	ε_0	ε_∞	α
313 K (40 ℃)	31.77	5.56	0.44
333 K (60 ℃)	45.54	5.51	0.48
353 K (80 ℃)	50.71	5.53	0.48

2.4　Complex impedance analysis

The increase of dielectric loss and dielectric permittivity at higher temperature is due to the conductivity increase of the sample. To understand this dielectric relaxation and analyze dynamics of the ionic movement in crystal, the complex impedance (Z'-Z'') plot at different temperature was made (Fig.7a). The plot shows a single semicircle for selected temperature related to bulk effects. It indicates that single conductivity process take place in the sample. These impedance plots were solved by fitting using equivalent circuit where each impedance semicircle can be represent by a resistor, R, and capacitor, C, in parallel. It is clearly seen from the Fig.7a that the radius of semicircle decreases with increasing temperature, which indicates that the decrease of the bulk resistance with an increases of the temperature. The temperature dependent conductivities σ_{dc} are plotted in the form of $\lg\sigma_{dc}$ versus 1 000/T, as shown in Fig.7b, the $\lg\sigma_{dc}$ as a function of 1 000/T shows linear relationship in the temperature range of 403~473 K, and the activation energy (E_{dc}) was estimated as 0.57(2) eV, which is similar with the activation energy obtained from dielectric relaxation. The similar active energy implies that charge carrier has to overcome the same energy barrier while conducting as well as relaxation. The conduction of **1** due to a process of charge transfer between the cation and anion. From

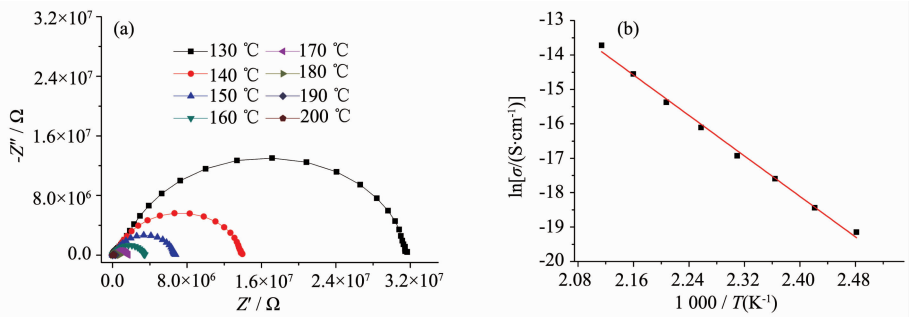

Fig.7 Complex-plane impedance plots for **1** at various temperatures(a) and temperature dependence of σ_{dc} for **1**(b) (Black dot: obtained from using an equivalent circuit; lines: theoretically reproduced)

the single crystal structure, there are diverse weak interactions between the anion and cation. As the temperature increasing, the motion of the alkyl chain of the cation induces the enhancement charge transfer and charge carrier. The motion of charge carriers in the low-mobility solids is accompanied by an electric relaxation. The charge transfer between the cation and anion is accompanied by the change in the direction of the dipole movement in the samples.

3 Conclusions

In summary, a molecular magnetic based on $[Ni(mnt)_2]^-$ spin system have been synthesized and characterized structurally via incorporating the easily mobile organic cation. Some weakly charge-assisted interactions between the mobile organic cation and rigid $[Ni(mnt)_2]^-$ anion were observed in the crystal structure of **1**. The dielectric results indicated that the dielectric relaxation in the investigated frequency range originates from the dynamic orientation motion of alkyl chain of the organic cation. The overall magnetic behavior of **1** corresponds to a paramagnetic system with ferromagnetic coupling interaction. This study provided a new strategy for the design of relax-like dielectric.

References:

[1] Wojnarowska Z, Knapik J, Diaz M, et al. *Macromolecules*, **2014**,**47**:4056-4065

[2] Arik E, Altan H, Esenturk O. *J. Phys. Chem. A*, **2014**,**118**: 3081-3089

[3] Xiao B, Zheng W, Dong Y L, et al. *J. Phys. Chem. C*, **2014**, **118**:5802-5809

[4] Moynihan C T. *Solid State Ionics*, **1998**,**105**:175-180

[5] Petrovsky V, Manohar A, Dogan F. *J. Appl. Phys.*, **2006**,**100**: 014102(2 pages)

[6] Sheoran A, Sanghi S, Rani S, et al. *J. Alloys Compd.*, **2009**, **475**:804-809

[7] Roling B, Happe A, Funke K, et al. *Phys. Rev. Lett.*, **1997**, **78**:2160-2163

[8] Ang C, Yu Z, Jing Z, et al. *Phys. Rev. B*, **2000**,**61**:3922 -3926

[9] Thongbai P, Yamwong T, Maensiri S. *Solid State Commun.*, **2008**,**147**:385-387

[10]Pradhan D K, Choudhary R N P, Samantaray B K. *Int. J. Electrochem. Sci.*, **2008**,**3**:597-608

[11]Xu G C, Ma X M, Zhang L, et al. *J. Am. Chem. Soc.*, **2010**,**132**:9588-9590

[12]ZHOU Qin-Qin(周琴琴), FU Da-Wei (付大伟). *Chinese J. Inorg. Chem.*(无机化学学报), **2013**,**29**(8):1696-1702

[13]Akutagawa T, Koshinaka H, Sato D, et al. *Nat. Mater.*, **2009**,**8**:342-347

[14]Fu D W, Cai H L, Liu Y M, et al. *Science*, **2013**,**339**:425-428

[15]Fu D W, Song Y M, Wang G X, et al. *J. Am. Chem. Soc.*, **2007**,**129**:5346-5347

[16]Fu D W, Dai J, Ge J Z, et al. *Inorg. Chem. Commun.*, **2010**, **13**:282-285

[17]Rodríguez-Molina B, Pérez-Estrada S, Garcia-Garibay M A, *J. Am. Chem. Soc.*, **2013**,**135**:10388-10395

[18]Jiang X, Rodríguez-Molina B, Nazarian N, et al. *J. Am. Chem. Soc.*, **2014**,**136**:8871-8874

[19]Kottas G S, Clarke L I, Horinek D, et al. *Chem. Rev.*, **2005**, **105**:1281-1376

[20]Kaszynski P, Friedli A C, Michl J. *J. Am. Chem. Soc.*, **1992**,**114**:601-620

[21]Winston E B, Lowell P J, Vacek J, et al. *Phys. Chem. Chem. Phys.*, **2008**,**10**:5188-5191

[22]Duan H B, Chen X R, Yang H, et al. *Inorg. Chem.*,

2013,**52**:3870-3877

[23]ZHOU Hong(周宏), YU Shan-Shan(于姗姗), DUAN Hai-Bao(段海宝), et al. *Chinese J. Inorg. Chem.*(无机化学学报), **2013**,**29**(7):1-10

[24]Duan H B, Ren X M, Meng Q J. *Coord. Chem. Rev*., **2010**, **254**:1509-1522

[25]Daun H B, Ren X M, Shen L J, et al. *Dalton Trans*., **2011**,**40**:3622-3630

[26]Davison A, Holm H R. *Inorg. Synth*., **1967**,**10**:8-26

[27]XU Duo-Hui(许多慧), SHENG Xiao-Li(盛小利), LU Chang-Sheng(芦昌盛), et al. *Chinese J. Inorg. Chem.* (无机化学学报), **2012**,**28**(5):888-892

[28]*SMART* and *SAINT*, Siemens Analytical X-ray Instrument Inc., Madison, WI, **1996**.

[29]Sheldrick G M. *SHELX*-97, *Program for the Refinement of Crystal Structure*, University of Göttingen, Germany, **1997**.

[30]wiergiel J, Jadzyn J. *Ind. Eng. Chem. Res*., **2011**,**50**:11935-11941

[31]Duan H B, Zhang X M, Zhou H. *Synth. Met*., **2014**,**15**:294-298